Novel RANKL DE-loop mutants antagonize RANK-mediated osteoclastogenesis

Wang, Yizhou; van Assen, Aart H G; Dos Reis, Carlos Ricardo Rodrigues; Setroikromo, Rita; van Merkerk, Ronald; Boersma, Ykelien L; Cool, Robbert H.; Quax, Wim J

Published in:
Febs Journal

DOI:
10.1111/febs.14142

The FEBS Journal

FEBS PRESS science publishing by scientists

Novel RANKL DE-loop mutants antagonize RANK-mediated osteoclastogenesis

Yizhou Wang†, Aart H.G. van Assen†, Carlos R. Reis, Rita Setroikromo, Ronald van Merkerk, Ykelien L. Boersma, Robbert H. Cool and Wim J. Quax

Department of Chemical and Pharmaceutical Biology, Groningen Research Institute of Pharmacy, University of Groningen, The Netherlands

Keywords
antagonist; bone homeostasis; osteoporosis; RANK; RANKL

Correspondence
W. J. Quax, Department of Chemical and Pharmaceutical Biology, Groningen Research Institute of Pharmacy, University of Groningen, A. Deusinglaan 1, 9713 AV Groningen, The Netherlands
Fax: +31 50 363 3000
Tel: +31 50 363 2558
E-mail: w.j.quax@rug.nl

†Both authors equally contributed to this manuscript

(Received 26 January 2017, revised 12 May 2017, accepted 14 June 2017)

doi:10.1111/febs.14142

Bone is a dynamic tissue that is maintained by continuous renewal. An imbalance in bone resorption and bone formation can lead to a range of disorders, such as osteoporosis. The receptor activator of NF-κB (RANK)–RANK-ligand (RANKL) pathway plays a major role in bone remodeling. Here, we investigated the effect of mutations at position I248 in the DE-loop of murine RANKL on the interaction of RANKL with RANK, and subsequent activation of osteoclastogenesis. Two single mutants, RANKL I248Y and I248K, were found to maintain binding and have the ability to reduce wild-type RANKL-induced osteoclastogenesis. The generation of RANK-antagonists is a promising strategy for the exploration of new therapeutics against osteoporosis.

Introduction

Bone is a dynamic tissue that has multiple functions, including support of muscles, protection of vital organs, and fostering hematopoietic marrow [1,2]. Under normal conditions, bone homeostasis is achieved by continuous renewal, mediated by two processes: bone resorption by osteoclasts and bone formation by osteoblasts [3]. An imbalance in bone resorption and formation can cause bone-associated diseases: when the activity of osteoclasts exceeds that of osteoblasts, osteoporosis will be developed. In contrast, osteopetrosis will occur when osteoblastic activity exceeds [4].

Osteoclastogenesis is regulated by a cytokine system, consisting of three major proteins: receptor activator of nuclear factor-κB (RANK), RANK-ligand (RANKL), and osteoprotegerin (OPG) [5]. The binding between RANKL on the surface of osteoblast cells and the RANK on osteoclast precursor cells will trigger activation of several transcription factors and enzymes that induce osteoclast maturation and bone resorption. OPG is a soluble decoy receptor, acting as a natural antagonist of RANKL [6]. The RANK–RANKL pathway plays an important role in both physiological and pathological bone development. Therefore, this signaling pathway is a promising target in bone-related diseases [3].

Receptor activator of nuclear factor-κB-ligand is a member of the tumor necrosis factor (TNF)-superfamily,

Abbreviations
mRANK, murine RANK; mRANKL, murine RANK-ligand; OPG, osteoprotegerin; RANKL, receptor activator of nuclear factor-κB-ligand; RANK, receptor activator of nuclear factor-κB; sfGFP-RANKL, superfolder green fluorescent protein-RANKL fusion protein; SPR, surface plasmon resonance; TNF, tumor necrosis factor; TNF-α, tumor necrosis factor α; TNF-R1, tumor necrosis factor receptor 1; TNF-R2, tumor necrosis factor receptor 2; TRAIL, tumor necrosis factor-related apoptosis-inducing ligand.

a group of cytokines involved in cell proliferation and cell death [7]. The TNF-superfamily consists of 19 multimeric ligands interacting with cognate receptor molecules; most of them require trimerization to initiate their signaling cascade [8]. Ligands belonging to the TNF-superfamily are mostly type II transmembrane glycoproteins, containing a C-terminal, receptor-interacting ectodomain, a transmembrane domain, and an N-terminal intracellular tail [4]; the extracellular domain can be either cleaved off by the proteolytic activity of metalloproteases or produced by alternative splicing [9,10].

Three-dimensional structures of TNF-α, TRAIL, and RANKL alone and in complex with their respective receptors have revealed very similar overall structures that comprise unique conserved elements involved in receptor binding [11–18]. One of these elements is the so-called DE-loop. There is a conserved tyrosine in the DE-loop of all TNF-ligands, with the exception of an arginine in CD40L and an isoleucine in RANKL. Interestingly, variants of human TNF-α with mutated DE-loop residues including the semiconserved residue Y87 were shown to be receptor antagonists: some mutants selectively bound to human TNF-receptor 1 (TNF-R1) and not TNF-receptor 2 (TNF-R2), while inhibiting wild-type TNF-α-mediated effects via TNF-R 1 [13]. Comparing the 3D structure of the antagonistic TNF-R1-selective mutant with that of wild-type TNF-α, it was concluded that the Y87H mutation changed the binding mode of the DE-loop to TNF-R1 from a hydrophobic to an electrostatic interaction [13]. In murine RANKL, mutation of the equivalent residue I248 to aspartate resulted in an eightfold lower ED_{50} [12]. In contrast, another 3D structure has led to the suggestion that the DE-loop may not be critical for mRANKL–mRANK binding [11,19].

Here we have investigated the effect of mutations of the I248 residue in the mRANKL DE-loop on the binding to mRANK and on subsequent osteoclastogenesis. Our results show that RANKL mutants I248Y and I248K have the ability to reduce RANKL-induced osteoclastogenesis. Thus, mutagenesis at position I248 of the DE-loop region can form the basis of a general strategy to create RANK-antagonists for the RANKL–RANK pathway, paving the way to novel osteoporosis treatments.

Results

In silico mutagenesis of mRANKL demonstrates importance of position I248

Several 3D structures of mRANKL have been described previously [4,11,12,20,21]. The 3D structure of mRANK in complex with mRANKL (Protein Data Bank accession code 4GIQ) was used for *in silico* mutagenesis at position I248 in order to estimate differences in $\Delta\Delta G_i$ binding to RANK between RANKL mutants and wild-type RANKL (WT RANKL) (Fig. 1A,B). A similar strategy has allowed us in the past to successfully generate variants of hTRAIL with desired properties, such as enhancement of affinity and change of receptor selectivity [22–24]. As shown in Fig. 1B, the RANK residues surrounding I248 of RANKL are hydrophilic, including D49, T50, N52, E53, and E54, suggesting that the surface interaction between the DE-loop of RANKL and RANK is predominantly hydrophilic. This is different from the binding between TNF and TNF-R1, where Y87 of TNF is buried in a hydrophobic 'pocket' of the TNF-R1. The importance of RANKL residue I248 for the interaction with RANK was investigated by *in silico* mutagenesis. The effects of variation at position 248 of RANKL on the calculated $\Delta\Delta G_i$ are shown in Fig. 1C. Overall, our data indicate that substitution by other amino acids results in a strong effect on binding of RANKL to RANK, either positive or negative, suggesting that this residue is indeed important for binding. Given the overall estimated effects on binding energies between RANKL and RANK, we decided to focus on and construct a subset of RANKL mutants. I248Y was chosen because of the conserved tyrosine at the same position in the DE-loop of TNF-ligands and its calculated large difference in $\Delta\Delta G_i$ (Fig. 1C); I248K because this mutation also has a predicted large effect on the $\Delta\Delta G_i$, plus it is homologous to the arginine found at this position in TNF-ligand family member CD40L; and finally I248D was chosen as it was previously reported to have an eightfold lower ED_{50} compared to WT RANKL [12]. As the interaction between the DE-loop of RANKL and RANK is mainly hydrophilic, all the hydrophobic mutations including I248W were not taken into consideration.

RANKL mutations I248Y and I248K show increased binding affinity to RANK

After expression, purification, and characterization of WT RANKL and mutants, we determined their affinities to RANK by surface plasmon resonance (SPR). Using a CM4 sensor chip and a low density of RANK-Fc [< 60 response units (RU)], we were able to measure the interaction between one trimeric RANKL molecule binding to one RANK-Fc monomer [8]. Indeed, the sensorgrams for WT RANKL, I248Y, I248K, and I248D all show a ~ 1 : 1 binding ratio (varying between 0.9 and 1.2) (Fig. 2). Hence, the data

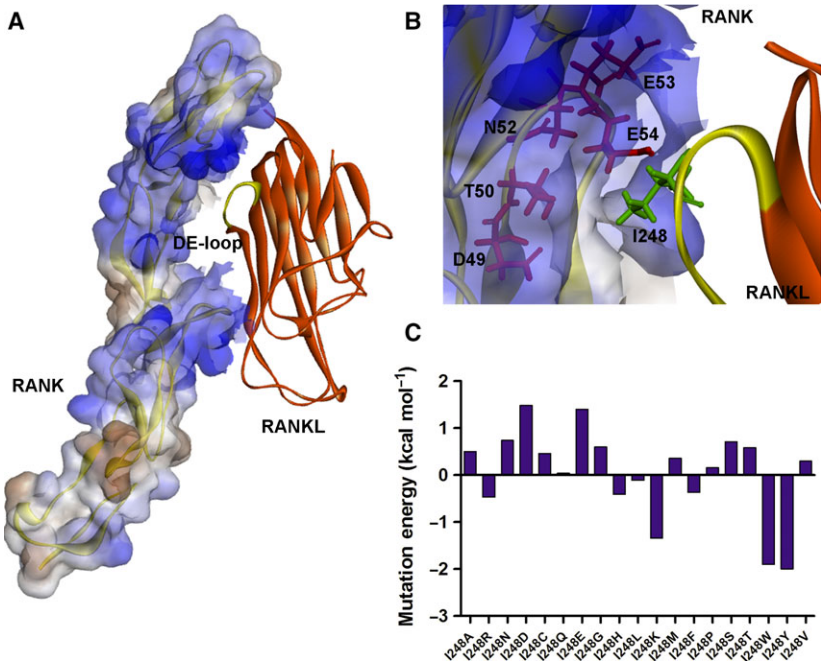

Fig. 1. Structural representation of the binding interface of the RANKL DE-loop with RANK and binding energy predictions for I248 mutants, made using Discovery Studio 4.5. (A) Refined structure of RANKL (orange) in complex with RANK (shown in hydrophilicity contact surface). The various strands and loops of RANKL are shown in orange and the DE-loop of RANKL is shown in yellow. The model was derived from the 3D structure of the murine RANKL–RANK complex (PDB code 4GIQ). (B) Detailed view of RANK residues in close proximity to residue I248 of RANKL. (C) Predicted differences in binding energy ($\Delta\Delta G_i$) of I248 variants binding to RANK when compared with WT RANKL. The change in energy is measured in kcal·mol^{-1}. A negative $\Delta\Delta G_i$ value indicates an improvement in receptor binding, whereas a positive $\Delta\Delta G_i$ value indicates a deterioration in receptor binding.

could be fitted with a 1 : 1 Langmuir fitting model and the kinetic parameters were calculated [8]. As shown in Table 1, I248Y and I248K showed approximately three- to fourfold higher affinities to the target receptor in comparison to WT RANKL. This was mainly caused by an increase in the association rate constant (k_a). The dissociation rate constants (k_d) of I248Y and I248K were comparable to WT RANKL. Mutant I248D showed a lower affinity to RANK-Fc compared to WT RANKL, which is mainly due to a much higher dissociation rate. Taken together, these results are consistent with the previous *in silico* predictions and they further confirm that the I248 residue indeed plays an important role in RANKL–RANK binding.

RANKL mutants compete for binding of WT RANKL to RANK and form high-order complexes with their receptor

To further assess whether the mutants compete with WT RANKL for binding, we performed a competitive ELISA assay, in which wells coated with RANK-Fc were incubated with both WT RANKL and RANKL variants. Our competitive ELISA results (Fig. 3) showed that increasing concentrations of both I248K and I248Y can efficiently compete with WT RANKL for RANK-Fc binding at physiological concentrations. However, RANKL I248D could only partially compete with WT RANKL at concentrations over 1000 nM, which is in accordance with the lowered affinity of RANKL I248D to RANK-Fc compared to WT RANKL.

Given that signaling of several TNF cytokines has been shown to require receptor oligomerization, we also tested whether mutants I248Y, I248K, and I248D could form multimeric complexes with RANK using high densities of RANK-Fc in SPR. As shown in Fig. 4, using the number of RU of bound RANK-Fc, we could estimate the ratio of complex formation (the number of trimeric RANKL units bound to monomeric RANK-Fc) using equation 1 (see Experimental Procedures). A binding ratio of 1 : 3.07 ± 0.01 was found for WT RANKL. For RANKL mutants I248Y, I248K, and I248D, mean binding ratios were 1 : 3.03 ± 0.04, 1 : 2.99 ± 0.02, and 1 : 3.12 ± 0.01, respectively. These results imply that the mutants, as WT RANKL, form a trimer–trimer complex with the RANK receptor.

RANKL mutants antagonize the biological activity of WT RANKL

We next tested the effect of RANKL mutants I248D, I248K, and I248Y on osteoclastogenesis by assessing their ability to induce multinucleation (three or more nuclei per cell) in osteoclast precursor murine RAW 264.7 cells and by testing their capability to inhibit WT RANKL (Fig. 5A, and Tables S1 and S2). Microscope photographs of osteoclasts from different

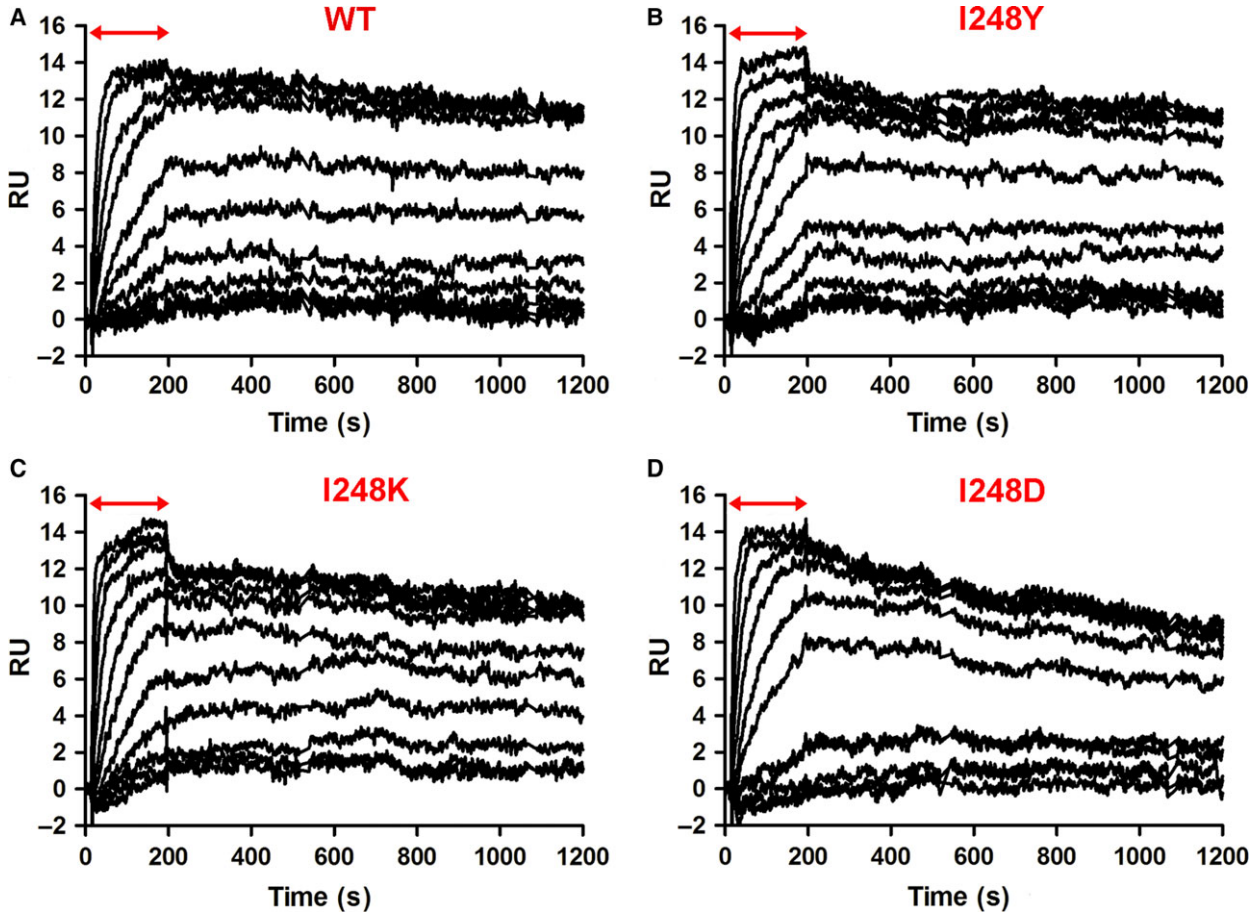

Fig. 2. Typical SPR sensorgrams obtained for binding between RANK-Fc and RANKL variants. The sensorgrams are obtained at receptor density < 60 RU to establish a 1 : 1 binding ratio. Depicted are (A) WT RANKL, (B) RANKL variant I248Y, (C) RANKL variant I248K, and (D) RANKL variant I248D. Injection of RANKL (0–20.48 nM) is marked with a double-headed arrow. After injection a buffer effect is visible for the higher concentrations used. Dissociation is followed up for 1000 s.

Table 1. Binding kinetics of the RANKL variants and WT RANKL to murine RANK-Fc as measured by surface plasmon resonance.

	$k_a \cdot 10^{-6}$ ($M^{-1} \cdot s^{-1}$)	$k_d \cdot 10^4$ (s^{-1})	K_D (pM)
WT	4.3 ± 1.5	1.5 ± 0.4	38 ± 2
I248Y	15.7 ± 7.7	1.3 ± 0.7	8 ± 3
I248K	17.1 ± 1.1	1.5 ± 0.4	9 ± 2
I248D	8.0 ± 0.9	4.2 ± 0.6	53 ± 7

treatments with RANKL variants (50 $ng \cdot mL^{-1}$) only, WT RANKL (50 $ng \cdot mL^{-1}$), or a combination of both are shown in Fig. 5A. Single treatment with WT RANKL caused osteoclast formation to a large extent and induced formation of giant multinucleated cells (two or more clusters of multinuclei per cell) which can cover large areas of the wells. RANKL variants themselves were also capable of inducing osteoclast formation, although the number of osteoclasts formed was lower than that induced by WT RANKL. Competition of either RANKL I248Y or I248K with 50 $ng \cdot mL^{-1}$ WT RANKL led to a reduction in both number and size of osteoclasts, while the competitive effect of RANKL I248D was less than that of I248Y and I248K. Importantly, single treatment with each of the three mutants induced less osteoclastogenesis compared to treatment with WT RANKL at all concentrations measured (Fig. 5B–D). The high-affinity mutants I248Y and I248K reached a maximum level at approximately 50 $ng \cdot mL^{-1}$, which is 70 and 80% of that of WT RANKL, respectively (Fig. 5B,C). In contrast, the low-affinity mutant I248D only reached up to 40% of the osteoclastogenic effect of WT RANKL even at the highest concentration of 150 $ng \cdot mL^{-1}$ (Fig. 5D). Cotreatment of RAW 264.7 cells with WT RANKL and high-affinity mutants I248Y or I248K led to a reduction in the level of osteoclastogenesis by 30–40% already at low concentration of mutant RANKL, with

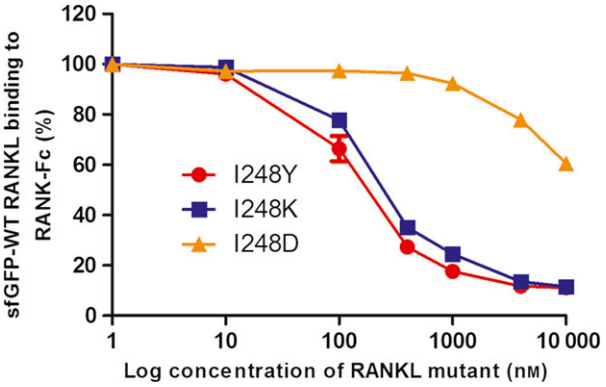

Fig. 3. Competitive ELISA performed with 10 nM sfGFP-WT RANKL and increasing concentrations (0–8000 nM) of variants I248Y (red circles), I248K (blue squares), and I248D (orange triangles). Bound sfGFP-WT RANKL was detected by incubation with a murine anti-GFP antibody and a secondary anti-mouse HRP-conjugated antibody. The signal was quantified using the One-step Turbo TMB reagent and absorbance was measured at 450 nm using a spectrophotometer. The percentage of sfGFP-WT RANKL bound was measured relative to the binding of 10 nM sfGFP-WT RANKL alone. The log concentration of the RANKL variants is displayed on the *x*-axis. The error bars reflect the standard deviation (SD) of three independent experiments.

no further reduction at higher concentrations (Fig. 5B, C). In contrast, the low-affinity mutant I248D only showed a reduction of the osteoclastic potential of WT RANKL at high concentrations (> 50 ng·mL^{-1}) (Fig. 5D).

Does exchange of RANKL subunits play a role in inhibition of WT RANKL-induced osteoclastogenesis?

In our studies, we showed inhibition of WT RANKL-induced osteoclastogenesis in the murine RAW 264.7 cell line by RANKL variants I248K and I248Y (Fig. 5). Although they themselves can also cause osteoclast formation, the numbers of osteoclasts are lower than those of WT RANKL (50 ng·mL^{-1}). The increased affinities of these mutants can explain the results of the inhibition experiments: both mutants showed higher affinities to RANK-Fc than WT RANKL (Fig. 2), which can make them compete efficiently with WT RANKL to occupy RANK and induce less osteoclastogenesis. An alternative explanation may be that the subunits of RANKL are interchanged, allowing formation of heterotrimeric RANKL molecules that are no longer able to activate RANK. To confirm or refute this hypothesis, we mixed purified sfGFP-WT RANKL with WT RANKL at equimolar ratio and incubated this for either 24 h at 37 °C or 44 h at 4 °C. The protein samples were loaded onto a size exclusion column while the absorbance was followed at 280 and 475/488 nm (Fig. 6). The trimeric fusion protein sfGFP-WT RANKL with its higher molecular weight eluted at approximately 12 mL showing absorbance at both wavelengths, whereas WT RANKL eluted at approximately 14.8 mL, showing only absorbance at 280 nm. Mixing of the two trimeric proteins did not result in shifting peaks, demonstrating that no exchange occurred during the incubation (Fig. 6).

Discussion

Bone homeostasis is achieved by continuously renewing the tissue [6]. Loss of bone remodeling homeostasis can lead to a range of disorders, including osteoporosis [6], bone lesions associated with rheumatoid arthritis [25], Paget's disease [26], and malignancy-induced bone diseases [27]. Due to the important role of the RANK–RANKL pathway in the bone remodeling process [5], interfering with their interaction is a promising strategy for therapeutic intervention. Initially, OPG-Fc was developed as a RANKL scavenger [28]; as OPG cross reacts with TRAIL, recently OPG variants lacking TRAIL binding were developed, showing significantly reduced osteoclastogenesis [29]. RANKL-targeted peptides were also developed and confirmed to prevent bone loss and inflammation in rheumatoid arthritis *in vivo* [19,30]. Finally, denosumab, an FDA-approved RANKL-specific antibody, was developed and is currently used in the treatment of osteoporosis and bone metastases [19]. Denosumab inhibits osteoclastogenesis by scavenging RANKL thus inhibiting receptor interaction. In contrast, we focused on novel RANKL variants, which will be of interest as these are blocking the receptor directly.

Three-dimensional structures of TNF-TNF-R1 and TRAIL-DR5 complexes show a conserved tyrosine residue in the DE-loop of ligands, which induces a hydrophobic interaction with loop 1 of the receptors [15,31]. Mukai *et al.* [32] created a series of receptor-selective TNF-α mutants with full bioactivity by using the phage display technique; the results showed that all active TNF-R1-selective mutants retained Y87, suggesting that Y87 is an essential residue for receptor binding. Furthermore, TNF-α mutation Y87H was generated as a part of a TNF-R1-selective antagonist, and Y87H was found to change the binding mode of the DE-loop from a hydrophobic to an electrostatic interaction [13]. *In silico* calculation of the effects of mutations of RANKL residue I248, which is homologous to TNF-α Y87, on the interaction with its

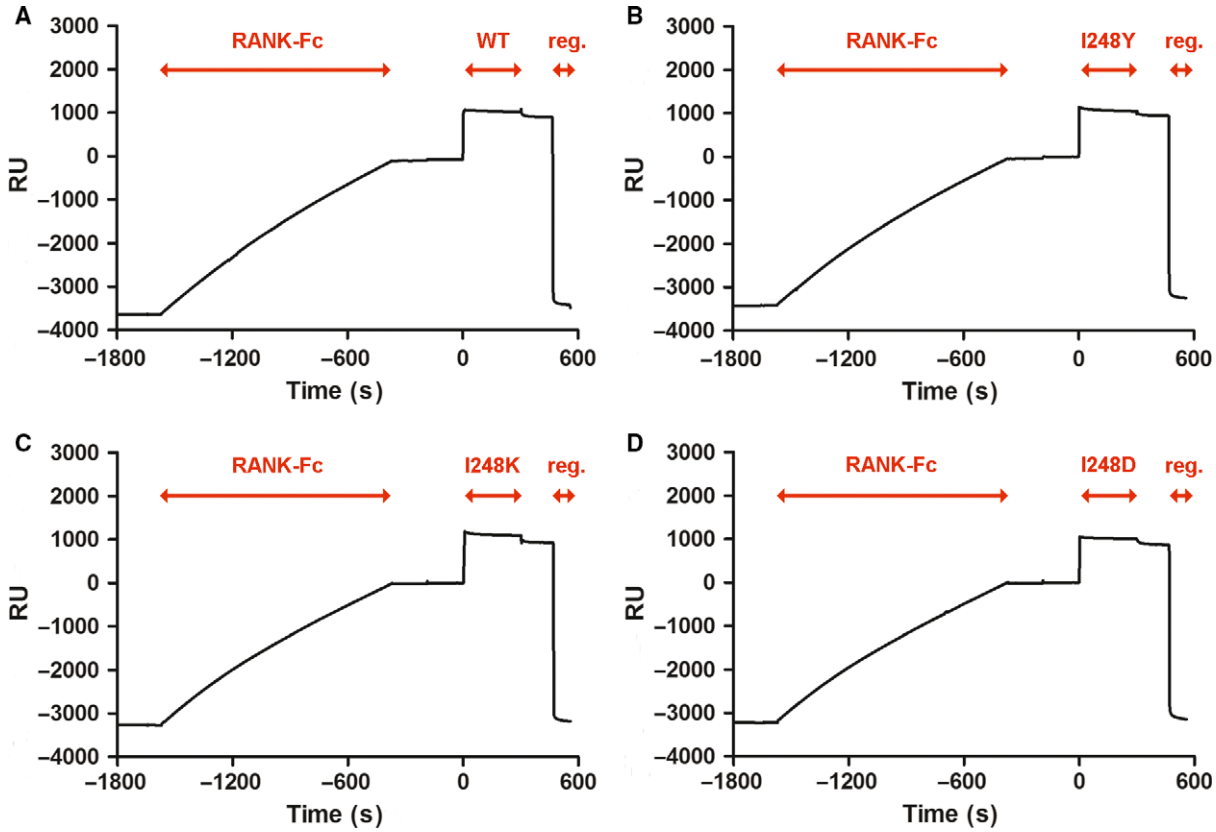

Fig. 4. Typical SPR sensorgrams to check trimer–trimer binding of RANKL and RANK-Fc. Depicted are the injection phases of RANK-Fc followed by the injection phase of WT RANKL or mutants. Regeneration (reg.) is visible at the end. With the number of response units (RU) bound, the ratio of complex formation, i.e., the number of trimeric RANKL units bound to monomeric RANK-Fc was estimated. Shown are the injections of (A) WT RANKL, (B) I248Y, (C) I248Y, and (D) I248D, leading to binding to RANK-Fc.

receptor RANK, suggested that mutagenesis of the I248 residue of RANKL has strong effect on binding of RANKL to RANK.

We have focused on three mutations on position 248: I248Y, I248K, and I248D. Detailed analysis of the interaction of RANKL proteins with RANK using SPR showed an increased affinity for mutants I248K and I248Y and a decreased affinity for I248D (Fig. 2 and Table 1). In accordance, competitive ELISA confirmed that RANKL I248Y and I248K can efficiently compete with WT RANKL for binding to RANK, whereas I248D cannot (Fig. 3). In line with these results, structural analysis of the impact of these mutations shows that the positively charged lysine on position 248 may interact with the negatively charged E54 residue on the RANK surface. Mutation I248Y could also result in an extra hydrogen bond and strengthened van der Waals forces, also reinforcing the binding of RANKL and RANK. The lower affinity for RANK that we measured for I248D can be explained by an electrostatic repulsion with E54 residue in RANK.

High-affinity mutants RANKL I248Y and I248K are still able to induce osteoclastogenesis but to a 20–30% lower maximum than WT RANKL, whereas low-affinity mutant I248D does not even reach 40% of this maximum activation level even at 150 ng·mL^{-1} (Fig. 5). Interestingly, the high-affinity mutants were able to reduce WT RANKL-mediated osteoclastogenesis already at low concentrations, whereas I248D shows a dose-dependent reduction of the WT RANKL signal up to the concentration of 150 ng·mL^{-1} (Fig. 5). All three mutants showed higher association rate constants (Table 1) allowing them to bind faster to the receptor than WT RANKL. Although high-affinity mutants I248K and I248Y have similar dissociation rate constants as WT RANKL, low-affinity mutant I248D has a higher dissociation rate constant (Table 1). The latter one leads to a less stable complex with RANK, which can explain why this mutant in itself is not very biologically active and why it reduces WT RANKL activity only at high concentrations (Fig. 5D). A similar explanation was formulated for antagonistic TNF-α mutation Y87H [13].

Our RANKL mutants can reduce WT RANKL activity by competing in binding to RANK, resulting in a reduction in biological activity to the level of the mutants themselves. What could be an explanation for this lower biological activity? In a molecular dynamics study on binding between TNF-ligand family member TRAIL and its death receptor DR5, Wassenaar *et al.* [33] proposed that through binding to TRAIL the conformational freedom of extracellular binding domains of DR5 was strongly restricted; this might also influence the stability of the intracellular death complex. Furthermore, Neumann *et al.* [34] showed that the signaling capabilities of the death receptors DR4 and DR5 do not only depend on binding of TRAIL but the transmembrane domains together with their adjacent stalk regions also control the signaling strength. Likewise, the transmembrane domain and adjacent extracellular stalk regions of RANK could play a similar role. RANKL may also play a role in controlling the conformational freedom of the extracellular domains of RANK. Mutants RANKL I248Y and I248K may slightly change the conformation of the RANKL–RANK complex, thus influencing the conformational freedom of RANK extracellular domains and subsequently the orientation of intracellular domains, which further influences the recruitment of downstream effector proteins.

In conclusion, our data show that the DE-loop is of importance for osteoclastogenesis and can be explored for the creation of new ligands with inhibitory properties. Given the importance of the DE-loop for RANK–RANKL signaling, the newly created mutants I248Y and I248K can form a starting point for novel therapeutic proteins in new osteoporosis treatments.

Experimental procedures

In silico calculations of the interaction energy of RANK in complexes with RANKL I248 mutants

Simulations were performed using the available 3D structure of murine RANKL in complex with RANK (Protein Data Bank accession code 4GIQ) [4]. All calculations and predictions were performed using BIOVIA Discovery studio 4.5. Briefly, the structures of RANKL and the I248 mutants were refined using the CHARMm force field. For the minimization of the receptor–ligand complex, the Smart Minimizer was used with maximum steps of 2000 and RMS gradient of 0.1, and Generalized Born with molecular volume (GBMW) was used as implicit solvation model. Predicted differences in RANK-binding energy ($\Delta\Delta G_i$) of the RANKL I248 mutants compared to WT RANKL were determined through interaction energy calculation. The change in energy was calculated in kcal·mol^{-1} and applies to a single binding interface. A negative $\Delta\Delta G_i$ value indicates an increase in receptor binding energy, whereas a positive $\Delta\Delta G_i$ value indicates a decrease in receptor binding energy.

Site-directed mutagenesis, production, and purification of the RANKL variants

cDNA encoding murine soluble RANKL (aa 160–316) was introduced in a pET15b expression plasmid (Novagen, Darmstadt, Germany) using the restriction sites *Nco*I and *BamH*I (Fermentas, St. Leon, Lithuania). Mutations at position 248 were introduced using megaprimers [35]. The PCR product was digested using *Dpn*I (Fermentas) to remove template DNA and used for transformation of *Escherichia coli* DH5α cells. Plasmid DNA was purified from an overnight culture (Nucleospin, Macherey-Nagel, Düren, Germany). After confirming the introduction of mutations by DNA sequencing, the plasmids were used for transformation of *E. coli* BL21(DE3). Transformants selected using ampicillin (Duchefa, Haarlem, the Netherlands) were grown overnight at 37 °C in 1 x LB medium (Tryptone, NaCl, and yeast extract all from Duchefa) containing 100 μg·mL^{-1} ampicillin. This culture was used to inoculate a larger culture (1 : 100 dilution), which was grown for approximately 2 h to OD_{600} 0.5, after which protein production was initiated by adding 1 mM IPTG (Duchefa), and continued for 16 h at 20 °C.

After harvesting cells by centrifugation and resuspending at 3 mL·g^{-1} wet cells in buffer A containing 50 mM MES pH 5.8 (Duchefa), 10% *v*/*v* glycerol (Duchefa), and 2 mM dithiothreitol (Sigma, Saint Louis, MO, USA), the cells were lysed by sonication. The RANKL proteins were mainly soluble. Supernatants were firstly loaded on a 5 mL cation exchange column (SP column, GE Healthcare,

Fig. 5. Relative number of osteoclasts obtained after treatment of murine RAW 264.7 cells with RANKL variants, WT RANKL or a combination of both. (A) Microscope images and absolute numbers of normal and giant osteoclasts from different treatments with RANKL variants (50 ng·mL^{-1}) only, WT RANKL (50 ng·mL^{-1}), or a combination of both at 200× magnification. The yellow bars represent the absolute numbers of normal osteoclasts, while the green bars represent the absolute numbers of giant osteoclasts; (B) Relative number of osteoclasts for variant I248Y compared to WT RANKL; (C) Relative number of osteoclasts for variant I248K compared to WT RANKL; (D) Relative number of osteoclasts for variant I248D compared to WT RANKL. The red bars represent the relative numbers of osteoclasts treated with RANKL variant alone, and the blue bars represent the combination treatment of RANKL variants with WT RANKL (50 ng·mL^{-1}). The number of osteoclasts in the well treated with 50 ng·mL^{-1} WT RANKL only was set to 100%. Significance was calculated using a Student's *t*-test compared to untreated cells: (*) is $P < 0.05$ and (**) is $P < 0.001$. The error bars reflect the SD of three independent experiments in triplicate. For WT RANKL alone, the error bar is the average SD over all separate experiments.

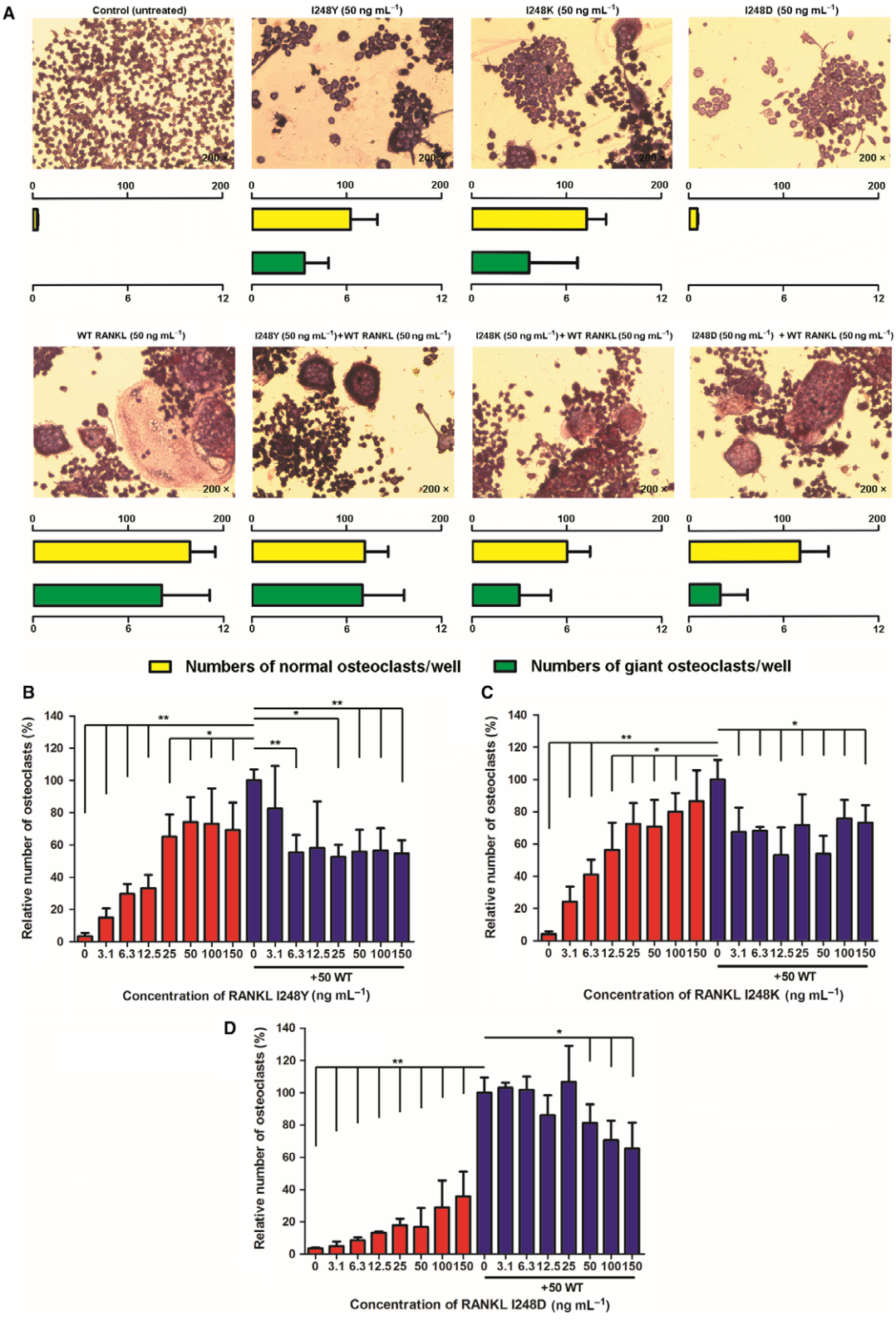

The FEBS Journal **284** (2017) 2501–2512 © 2017 The Authors. *The FEBS Journal* published by John Wiley & Sons Ltd on behalf of Federation of European Biochemical Societies.

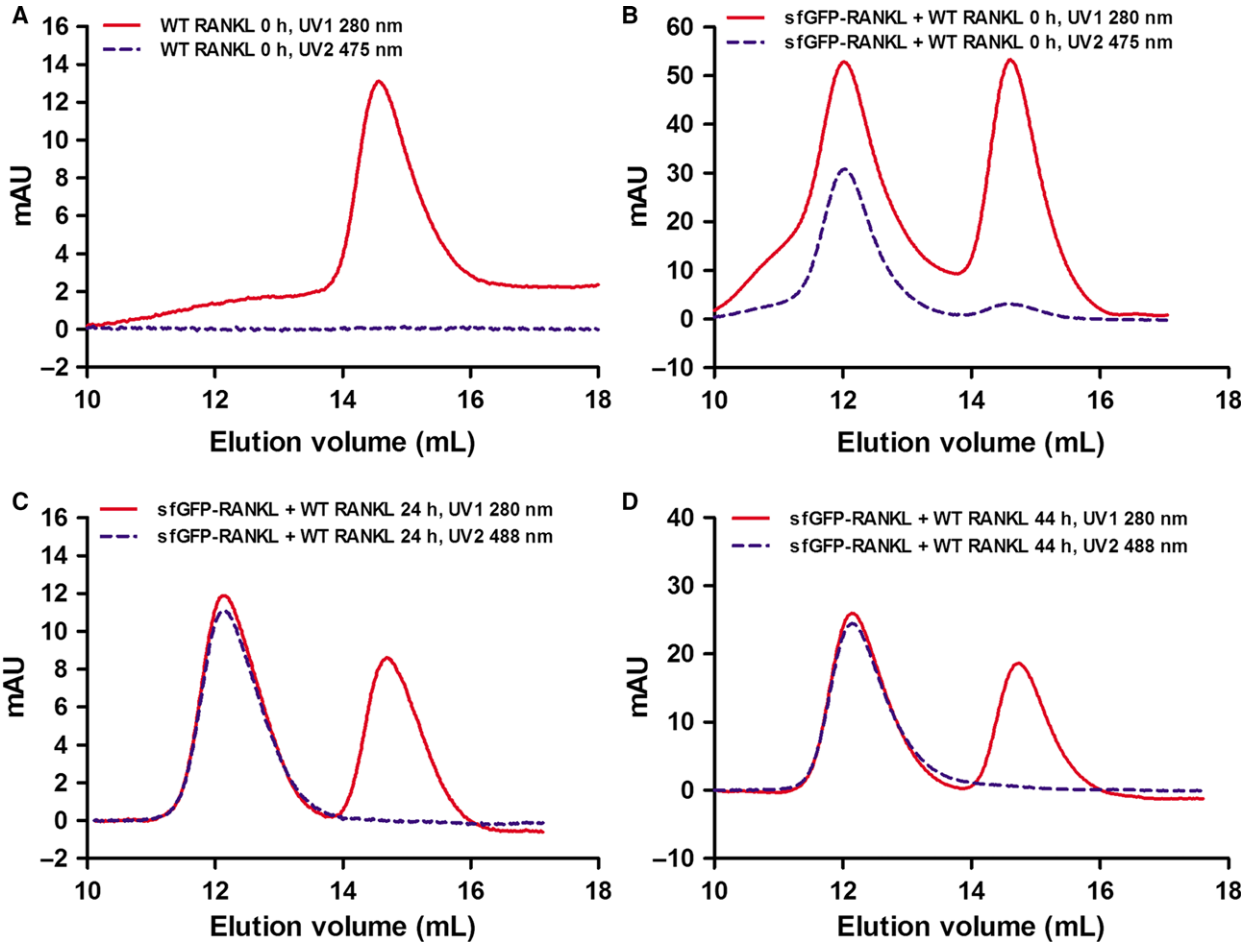

Fig. 6. Size exclusion chromatography for the determination of the potential exchange of RANKL subunits. (A) Chromatogram of WT RANKL at 0 h; (B) Chromatogram for a mixture of WT RANKL and sfGFP-WT RANKL at concentrations of 12 μM each at 0 h; (C) Chromatogram for a mixture of WT RANKL and sfGFP-WT RANKL after incubation for 24 h at 37 °C, and (D) for 44 h at 4 °C. Elution was monitored in mAU at 280 nm (all proteins), 475 nm, and 488 nm (sfGFP fusion proteins).

Uppsala, Sweden) using buffer A. Buffer B, similar to A but containing 2 M NaCl (Duchefa), was used to elute the protein. Elution of the fractions containing RANKL occurred with 300–400 mM NaCl. The presence of proteins was confirmed by western blotting using an anti-mRANKL antibody (R&D Systems, Minneapolis, MN, USA) and corresponding anti-goat-horse radish peroxidase (HRP) antibody (Biosource, Waltham, UK).

The obtained protein-containing fractions were pooled and loaded onto a HiLoad Superdex75 16/60 size exclusion chromatography column (GE Healthcare), using buffer A. The retention volumes of the RANKL proteins corresponded to the hydrodynamic radius of a trimeric complex. The proteins were checked by SDS/PAGE to determine the purity which was estimated to be more than 90% pure. Concentrations were determined with the Coomassie Bradford protein assay kit (Pierce, Rockford, IL, USA) using bovine serum albumin (BSA, ThermoScientific, Rockford, IL, USA) as a standard. The final yield of the variants was approximately 2 mg purified protein per liter culture. When calculating molarity, we used the molecular weight of trimeric RANKL proteins.

Superfolder green fluorescent protein was amplified from pQE30_sfGFP [36] by PCR, digested with *Nco*I/*Nco*I site and ligated into the vector pET15b_WT RANKL to encode sfGFP fused to the N terminus of WT RANKL. sfGFP-WT RANKL was produced in BL21(DE3) cells similar to our variants. For the purification of sfGFP-WT RANKL, cleared cell lysate was firstly loaded onto a 5 mL anion exchange column (Q column, GE Healthcare), using a buffer of 20 mM Tris pH 8.5, 2 mM dithiothreitol, and 10% *v*/*v* glycerol. Buffer B, similar to A but containing 2 M NaCl, was used to elute the protein. Elution of the fractions containing sfGFP-WT RANKL occurred at 300–500 mM NaCl. The obtained protein-containing fractions were pooled and loaded onto a 5 mL cation exchange column, followed by a

HiLoad Superdex200 16/60 size exclusion chromatography column (GE Healthcare), and the purification steps were similar with that of WT RANKL.

Kinetic analysis of complex formation between trimeric RANKL and monomeric RANK-Fc

Binding between RANKL and RANK-Fc was determined using a Biacore 3000 system (GE Healthcare). A CM4 chip was directly coated with 70 $\mu g \cdot mL^{-1}$ protein A (Sigma), making use of the amine coupling kit (GE Healthcare) according to the manufacturer's instructions. The amount of immobilized protein A was typically around 1000 RU. Next, murine RANK-Fc (R&D Systems) was captured at a low density, never exceeding 60 RU. The flow rate used for immobilization was 50 $\mu L \cdot min^{-1}$. RANKL was injected at a flow rate of 50 $\mu L \cdot min^{-1}$ in concentrations between 0.01 nM and 20.48 nM for 3 min. Dissociation of the formed complex was followed up for 1000 s. HBS-N buffer (GE Healthcare) with 0.005% *v*/*v* surfactant P20 (GE Healthcare, Uppsala, Sweden) was used as a running buffer. The chip surface was regenerated between cycles with two injections of 10 mM glycine (Duchefa) pH 1.5 for 30 s each. The responses were corrected for buffer effect and binding to the protein A chip surface [8]. At low receptor densities, the data could be fitted to a 1 : 1 Langmuir model using the BIAEVALUATION software version 4.2 (GE Healthcare) [8].

Determination of trimer–trimer complexes using SPR

To confirm whether a trimer–trimer complex could be formed between RANKL and RANK, an SPR experiment was set up as previously described [8]. RANK-Fc was captured at high density, > 1000 RU, on the surface of a CM5 chip by immobilized protein A. RANKL was injected at a high concentration of 5000 nM with a flow rate of 10 $\mu L \cdot min^{-1}$. After each cycle, the chip surface was regenerated as described above. With equation 1, the ratio of the complex formation, n, can be calculated by measuring the maximal response (R_{max}) that can be reached by formation of the complex AB_n between trimeric RANKL (A; with molecular weight MW_A = 52.7 kDa) and monomeric RANK-Fc (B; with molecular weight MW_B = 60 kDa) captured at density $RU_{captured}$ [8].

$$R_{max} = [MW_A/(n \cdot MW_B)] \cdot RU_{captured} \quad (1)$$

Competitive ELISA

Competition between selected RANKL mutants and WT RANKL was determined using a competitive enzyme-linked immunosorbent assay (ELISA). Murine RANK-Fc (Sigma) was immobilized on a 96-well Microlon 600 plate (Greiner, Frickenhausen, Germany) by incubating the wells with 25 nM RANK-Fc in 0.1 M $NaHCO_3$ (Merck, Darmstadt, Germany) buffer pH 8.6 overnight at 4 °C. Subsequently, the wells were washed with Tris-buffered saline (TBS) buffer including 0.05% *v*/*v* Tween 20 (TBST, Duchefa), pH 7.4, followed by a 2-h incubation at room temperature with 2% *w*/*v* BSA (Roche, Mannheim, Germany) in phosphate-buffered saline (PBS), pH 7.4. After washing with TBST buffer, the wells were incubated for 30 min at room temperature with the RANKL variants I248K, I248Y, and I248D at concentrations in the range of 0–8000 nM, mixed with 10 nM sfGFP-WT RANKL. After washing with TBST buffer, bound sfGFP-WT RANKL was detected by incubation with a murine anti-GFP antibody (Sigma) and a secondary anti-mouse HRP-conjugated antibody (Millipore, Billerica, MA, USA). The signal was quantified using the One-step Turbo TMB reagent (ThermoScientific) and absorbance was measured at 450 nm. The percentage of sfGFP-WT RANKL bound was measured relative to the binding of 10 nM sfGFP-WT RANKL alone.

Inhibition of osteoclastogenesis

Cells from the murine leukemic monocyte macrophage cell line RAW 264.7 were cultured as described before [37]. Cells were subcultured every third or fourth day using a 1 : 10 dilution in fresh Dulbecco's modified Eagle's medium (Life Technologies, Carlsbad, CA, USA) containing 10% *v*/*v* fetal calf serum (FCS, Life Technologies) and 2 mM penicillin/streptomycin (Life Technologies). Cells were seeded at a density of 1000 cells per well in a 96-well plate (Greiner). At day 3, the medium was changed to Alpha-MEM (Invitrogen, Carlsbad, CA, USA) containing 2 mM penicillin/streptomycin and 10% *v*/*v* FCS (Invitrogen); different concentrations of RANKL were added, ranging from 3.1 to 150 $ng \cdot mL^{-1}$. Inhibition of WT RANKL-induced osteoclastogenesis by RANKL mutants was assessed via treatment of RAW 264.7 cells with 50 $ng \cdot mL^{-1}$ WT RANKL and a concentration range (3.1–150 $ng \cdot mL^{-1}$) of a determined RANKL mutant. At day 5, the medium was exchanged, and both WT RANKL and RANKL mutants were added using the same concentrations as described for day 3. At day 7, osteoclastogenesis was determined using the tartrate resistance acid phosphatase (TRAP) assay (Sigma) according to the manufacturer's instructions. The number of osteoclasts in the wells containing 50 $ng \cdot mL^{-1}$ WT RANKL was set to 100%, and the number of osteoclasts in all other wells was calculated relative to this reference well. Multinucleated (three or more nuclei) TRAP-positive cells were considered as osteoclasts. Osteoclasts with two or more clusters of multinuclei were considered as giant osteoclasts.

Determination of exchange of RANKL subunits

The exchange of RANKL subunits was determined using size exclusion chromatography. WT RANKL and sfGFP-WT RANKL at concentrations of 12 μM were incubated

together in a 1 : 1 ratio for 24 h at 37 °C or for 44 h at 4 °C. After incubation, samples were loaded onto a Superdex 200 10/30 column (GE Healthcare) using buffer E (20 mM sodium phosphate buffer pH 7.4, 10% *v*/*v* glycerol,). Elution was monitored at 280 nm (all proteins) and at 475/488 nm (sfGFP-WT RANKL); the chromatograms were compared to that of a mixture of sfGFP-WT RANKL and WT RANKL at 0 h.

Acknowledgements

Murine RAW 264.7 cells were a kind gift from J. Doktor, Department of Pathology and Medical Biology, University Medical Center Groningen, Groningen, The Netherlands. This work was performed within the framework of the Dutch Top Institute Pharma project TNF-ligands in cancer (project nr. T3-112) and STW grant 11056. YW is a recipient of a scholarship from the Chinese Scholarship Council (CSC).

Author contributions

YW, AHGA, CRR, RS, RM, and RHC performed experiments and analyzed data. YLB, RHC, and WJQ planned the research and supervised the study. YW, AHGA, YLB, RHC, and WJQ wrote the paper.

References

1 Kim J & Kim N (2016) Signaling pathways in osteoclast differentiation. *Chonnam Med J* **52**, 12–17.
2 Boyce BF & Xing L (2007) Biology of RANK, RANKL, and osteoprotegerin. *Arthritis Res Ther* **9**, S1.
3 Tanaka S, Nakamura K, Takahasi N & Suda T (2005) Role of RANKL in physiological and pathological bone resorption and therapeutics targeting the RANKL-RANK signaling system. *Immunol Rev* **208**, 30–49.
4 Nelson CA, Warren JT, Wang MWH, Teitelbaum SL & Fremont DH (2012) RANKL employs distinct binding modes to engage RANK and the osteoprotegerin decoy receptor. *Structure* **20**, 1971–1982.
5 Trouvin AP & Goëb V (2010) Receptor activator of nuclear factor-κB ligand and osteoprotegerin: maintaining the balance to prevent bone loss. *Clin Interv Aging* **5**, 345–354.
6 Rachner T, Khosla S, Hofbauer L & Manuscript A (2011) New horizons in osteoporosis. *Lancet* **377**, 1276–1287.
7 Bodmer JL, Schneider P & Tschopp J (2002) The molecular architecture of the TNF superfamily. *Trends Biochem Sci* **27**, 19–26.
8 Reis CR, van Assen AHG, Quax WJ & Cool RH (2011) Unraveling the binding mechanism of trivalent tumor necrosis factor ligands and their receptors. *Mol Cell Proteomics* **10** (M110), 002808.
9 Walsh NC, Alexander KA, Manning CA, Karmakar S, Karmakar SK, Wang JF, Weyand CM, Pettit AR & Gravallese EM (2013) Activated human T cells express alternative mRNA transcripts encoding a secreted form of RANKL. *Genes Immun* **14**, 336–345.
10 Ikeda T, Kasai M, Utsuyama M & Hirokawa K (2001) Determination of three isoforms of the receptor activator of nuclear factor-kappaB ligand and their differential expression in bone and thymus. *Endocrinology* **142**, 1419–1426.
11 Liu C, Walter TS, Huang P, Zhang S, Zhu X, Wu Y, Wedderburn LR, Tang P, Owens RJ, Stuart DI *et al.* (2010) Structural and functional insights of RANKL-RANK interaction and signaling. *J Immunol* **184**, 6910–6919.
12 Lam J, Nelson CA, Ross FP, Teitelbaum SL & Fremont DH (2001) Crystal structure of the TRANCE/RANKL cytokine reveals determinants of receptor-ligand specifity. *J Clin Invest* **108**, 971–979.
13 Shibata H, Yoshioka Y, Ohkawa A, Minowa K, Mukai Y, Abe Y, Taniai M, Nomura T, Kayamuro H, Nabeshi H *et al.* (2008) Creation and X-ray structure analysis of the tumor necrosis factor receptor-1-selective mutant of a tumor necrosis factor-alpha antagonist. *J Biol Chem* **283**, 998–1007.
14 Luan X, Lu Q, Jiang Y, Zhang S, Wang Q, Yuan H, Zhao W, Wang J & Wang X (2016) Crystal structure of human RANKL complexed with its decoy receptor opsteoprotegerin. *J Immunol* **189**, 245–252.
15 Hymowitz SG, Christinger HW, Fuh G, Ultsch M, O'Connell M, Kelley RF, Ashkenazi A & de Vos AM (1999) Triggering cell death: the crystal structure of Apo2L/TRAIL in a complex with death receptor 5. *Mol Cell* **4**, 563–571.
16 Jones EY, Stuart DI & Walker NPC (1989) Structure of tumour necrosis factor. *Nature* **338**, 225–228.
17 Liang S, Dai J, Hou S, Su L, Zhang D, Guo H, Hu S, Wang H, Rao Z, Guo Y *et al.* (2013) Structural basis for treating tumor necrosis factor α (TNFα)-associated diseases with the therapeutic antibody infliximab. *J Biol Chem* **288**, 13799–13807.
18 Mongkolsapaya J, Grimes JM, Chen N, Xu XN, Stuart DI, Jones EY & Screaton GR (1999) Structure of the TRAIL-DR5 complex reveals mechanisms conferring specificity in apoptotic initiation. *Nat Struct Biol* **6**, 1048–1053.
19 Ta HM, Nguyen GTT, Jin HM, Choi J, Park H, Kim N, Hwang H-Y & Kim KK (2010) Structure-based development of a receptor activator of nuclear factor-kappaB ligand (RANKL) inhibitor peptide and molecular basis for osteopetrosis. *Proc Natl Acad Sci USA* **107**, 20281–20286.
20 Ito S, Wakabayashi K, Ubukata O, Hayashi S, Okada F & Hata T (2002) Crystal structure of the extracellular

domain of mouse RANK ligand at 2.2-Å resolution. *J Biol Chem* **277**, 6631–6636.
21 Ito S & Hata T (2004) Crystal structure of RANK ligand involved in bone metabolism. *Vitam Horm* **67**, 19–33.
22 Reis CR, Van der Sloot AM, Szegezdi E, Natoni A, Tur V, Cool RH, Samali A, Serrano L & Quax WJ (2009) Enhancement of antitumor properties of rhTRAIL by affinity increase toward its death receptors. *Biochemistry* **48**, 2180–2191.
23 Tur V, Van der Sloot AM, Reis CR, Szegezdi E, Cool RH, Samali A, Serrano L & Quax WJ (2008) DR4-selective tumor necrosis factor-related apoptosis-inducing ligand (TRAIL) variants obtained by structure-based design. *J Biol Chem* **283**, 20560–20568.
24 Van der Sloot AM, Tur V, Szegezdi E, Mullally MM, Cool RH, Samali A, Serrano L & Quax WJ (2006) Designed tumor necrosis factor-related apoptosis-inducing ligand variants initiating apoptosis exclusively via the DR5 receptor. *Proc Natl Acad Sci U S A* **103**, 8634–8639.
25 Mori H, Kitazawa R, Mizuki S, Nose M, Maeda S & Kitazawa S (2002) RANK ligand, RANK, and OPG expression in type II collagen-induced arthritis mouse. *Histochem Cell Biol* **117**, 283–292.
26 Whyte MP (2006) Paget's disease of bone and genetic disorders of RANKL/OPG/RANK/NF-kappaB signaling. *Ann N Y Acad Sci* **1068**, 143–164.
27 Lipton A, Uzzo R, Amato RJ, Ellis GK, Hakimian B, Roodman GD & Smith MR (2009) The science and practice of bone health in oncology: managing bone loss and metastasis in patients with solid tumors. *J Natl Compr Canc Netw* **7** (Suppl. 7), S1–S29; quiz S30.
28 Body J-J, Greipp P, Coleman RE, Facon T, Geurs F, Fermand J-P, Harousseau J-L, Lipton A, Mariette X, Williams CD *et al.* (2003) A phase I study of AMGN-0007, a recombinant osteoprotegerin construct, in patients with multiple myeloma or breast carcinoma related bone metastases. *Cancer* **97**, 887–892.
29 Higgs JT, Jarboe JS, Lee JH, Chanda D, Lee CM, Deivanayagam C & Ponnazhagan S (2015) Variants of osteoprotegerin lacking TRAIL binding for therapeutic bone remodeling in osteolytic malignancies. *Mol Cancer Res* **33**, 395–401.
30 Naidu VGM, Dinesh Babu KR, Thwin MM, Satish RL, Kumar PV & Gopalakrishnakone P (2013) RANKL targeted peptides inhibit osteoclastogenesis and attenuate adjuvant induced arthritis by inhibiting NF-κB activation and down regulating inflammatory cytokines. *Chem Biol Interact* **203**, 467–479.
31 Banner DW, D'Arcy A, Janes W, Gentz R, Schoenfeld HJ, Broger C, Loetscher H & Lesslauer W (1993) Crystal structure of the soluble human 55 kd TNF receptor-human TNFβ complex: Implications for TNF receptor activation. *Cell* **73**, 431–445.
32 Mukai Y, Shibata H, Nakamura T, Yoshioka Y, Abe Y, Nomura T, Taniai M, Ohta T, Ikemizu S, Nakagawa S *et al.* (2009) Structure-function relationship of tumor necrosis Factor (TNF) and its receptor interaction based on 3D structural analysis of a fully active TNFR1-selective TNF mutant. *J Mol Biol* **385**, 1221–1229.
33 Wassenaar TA, Quax WJ & Mark AE (2008) The conformation of the extracellular binding domain of Death Receptor 5 in the presence and absence of the activating ligand TRAIL: a molecular dynamics study. *Proteins* **70**, 333–343.
34 Neumann S, Bidon T, Branschädel M, Krippner-Heidenreich A, Scheurich P & Doszczak M (2012) The transmembrane domains of TNF-related apoptosis-inducing ligand (TRAIL) receptors 1 and 2 co-regulate apoptotic signaling capacity. *PLoS One* **7**, e42526.
35 Miyazaki K & Takenouchi M (2002) Creating random mutagenesis libraries using megaprimer PCR of whole plasmid. *Biotechniques* **33**, 1033–1034, 1036–1038.
36 Boersma YL, Chao G, Steiner D, Wittrup KD & Plückthun A (2011) Bispecific Designed Ankyrin Repeat Proteins (DARPins) targeting epidermal growth factor receptor inhibit A431 cell proliferation and receptor recycling. *J Biol Chem* **286**, 41273–41285.
37 Duan L, de Vos P, Fan M & Ren Y (2008) Notch is activated in RANKL-induced osteoclast differentiation and resorption. *Front Biosci* **13**, 7064–7071.

Supporting information

Additional Supporting Information may be found online in the supporting information tab for this article:

Table S1. Absolute numbers of normal and giant osteoclasts per RANKL treatment (experiment 1).

Table S2. Absolute numbers of normal and giant osteoclasts per RANKL treatment (experiment 2).